Monthly Notices of the ROYAL ASTRONOMICAL SOCIETY

MNRAS **452,** 2692–2699 (2015) doi:10.1093/mnras/stv1193

Counting quasar–radio source pairs to derive the millijansky radio luminosity function and clustering strength to $z = 3.5$

S. Fine,[1⋆] T. Shanks,[2] R. Johnston,[1] M. J. Jarvis[1,3] and T. Mauch[4]

[1]*Department of Physics, University of Western Cape, Bellville 7535, Cape Town, South Africa*
[2]*Department of Physics, Durham University, South Road, Durham DH1 3LE, UK*
[3]*Oxford Astrophysics, Denys Wilkinson Building, Keble Rd, Oxford OX1 3RH, UK*
[4]*SKA Africa, 3rd Floor, The Park, Park Road, Pinelands 7405, South Africa*

Accepted 2015 May 22. Received 2015 May 22; in original form 2015 January 28

ABSTRACT

We apply a cross-correlation technique to infer the $S > 3$ mJy radio luminosity function (RLF) from the NRAO VLA Sky Survey (NVSS) to $z \sim 3.5$. We measure Σ the over density of radio sources around spectroscopically confirmed quasars. Σ is related to the space density of radio sources at the distance of the quasars and the clustering strength between the two samples, hence knowledge of one constrains the other. Under simple assumptions we find $\Phi \propto (1+z)^{3.7\pm0.7}$ out to $z \sim 2$. Above this redshift the evolution slows and we constrain the evolution exponent to <1.01 (2σ). This behaviour is almost identical to that found by previous authors for the bright end of the RLF potentially indicating that we are looking at the same population. This suggests that the NVSS is dominated by a single population; most likely radio sources associated with high-excitation cold-mode accretion. Inversely, by adopting a previously modelled RLF we can constrain the clustering of high-redshift radio sources and find a clustering strength consistent with $r_0 = 15.0 \pm 2.5$ Mpc up to $z \sim 3.5$. This is inconsistent with quasars at low redshift and some measurements of the clustering of bright FR II sources. This behaviour is more consistent with the clustering of lower luminosity radio galaxies in the local Universe. Our results indicate that the high-excitation systems dominating our sample are hosted in the most massive galaxies at all redshifts sampled.

Key words: methods: statistical – galaxies: active – galaxies: evolution – galaxies: luminosity function, mass function – radio continuum: galaxies.

1 INTRODUCTION

The standard approach to measuring the radio luminosity function (RLF) requires a sample with distance information to convert fluxes to luminosities. These distances typically come from a cross-match to existing optical redshift surveys. Millijansky radio sources have sky densities of a few tens per square degree (Condon et al. 1998; Mauch et al. 2003) hence require wide-field ($\gtrsim 100$ deg^2) spectroscopic surveys to build up significant statistics in the RLF. These samples exist in the local Universe (e.g. 6dF, SDSS) and in combination with wide-field mJy radio catalogues the local RLF has been shown to be a combination of two main populations: active galactic nuclei (AGN) with a double power-law LF (similar to that of quasars e.g. Boyle et al. 2000) at high luminosities and star-forming galaxies with a Schechter function LF at lower luminosities (Best et al. 2005; Mauch & Sadler 2007).

Wide-field spectroscopic surveys are not deep enough to probe the overall galaxy population at higher redshift. Luminous red galaxies (LRGs) are bright enough to produce large samples up to $z \sim 0.7$ (Eisenstein et al. 2001; Cannon et al. 2006). While this is hardly a representative slice of the galaxy population, local surveys show that most radio sources in the $10^{24} < L < 10^{26}$ W Hz^{-1} regime (that translates to fluxes of $S \sim 1$–100 mJy at $z \sim 0.7$) are associated with massive red galaxies (Condon & Broderick 1988; Mauch & Sadler 2007). Using LRGs, Sadler et al. (2007) found evolution described well by shifting the AGN portion of the local RLF in the luminosity direction by $(1+z)^{2.0}$. These results were in broad agreement with Clewley & Jarvis (2004) who used galaxies from the Sloan Sigital Sky Survey (SDSS) to show that fainter $L < 10^{25}$ W Hz^{-1} sr^{-1} radio sources evolved more slowly than brighter ones up to $z \sim 0.5$.

Deep pencil-beam optical surveys offer higher redshift galaxy samples that, when combined with deep radio imaging, constrain the sub-mJy RLF. At these lower flux densities ($\lesssim 0.1$ mJy) radio surveys become dominated by star-forming galaxies (Seymour et al. 2008; Padovani et al. 2009) that show strong luminosity evolution $\propto (1+z)^{\sim 2.5}$ (Padovani et al. 2011; McAlpine, Jarvis & Bonfield

⋆ E-mail: s.lb.fine@gmail.com

2013), with some contribution from radio-quiet AGN (Jarvis & Rawlings 2004; Simpson et al. 2006). The lower luminosity AGN found in these surveys show somewhat less evolution than the Sadler et al. (2007) result. Padovani et al. (2011) find no evolution in their AGN to $z \sim 5$, and when they remove possible star formation derived emission they find negative evolution. They suggest this may be a result of extremely high-redshift objects in their sample and the RLF cutting off and declining for $z \gtrsim 1$–2. Below these extreme redshifts, Smolčić et al. (2009) and McAlpine et al. (2013) find slow but significant evolution in their AGN: $\propto (1+z)^{1.2}$ and $(1+z)^{0.8}$, respectively.

Small radio samples with complete spectroscopic coverage constrain the bright end of the RLF at high z (Dunlop & Peacock 1990; Willott et al. 2001). These studies show that at bright fluxes radio sources are found up to high-redshift ($z \sim 3$), indicating the difficulty in obtaining complete spectroscopy on large radio samples. They also found strong evolution in the RLF. Willott et al. (2001) used a combination of tiered radio samples with a faintest limit of $S_{151\,\mathrm{MHz}} > 500$ mJy to model the RLF. They separated their LF model into two populations roughly separated by being above or below $L \sim 10^{26}$ W Hz^{-1}. The lower luminosity population being primarily FR I objects or FR IIs that show little evidence for an AGN in the optical, and the higher luminosity sample containing bright FR II sources often associated with optical quasars. The brighter population's LF increases towards higher z peaking at $z \sim 2$ and then falling. The fainter end is described by a Schechter function that increases until it reaches $z \sim 1$ after which it remains stationary. In reality the lower luminosity population is poorly constrained for $z \gtrsim 1$ although further strong evolution is ruled out by source counts.

Above $z \sim 0.7$ the mJy RLF is difficult to constrain. It lies between the parameter spaces constrained by pencil-beam surveys that run out of radio sources at higher flux densities, and the targeted surveys that require large amounts of telescope time to push fainter. In this regime the RLF has been estimated from samples that have semicomplete spectroscopic coverage supplemented by photometric redshifts. Waddington et al. (2001) used a 1 mJy limited sample of 72 galaxies with 65 per cent spectroscopic completeness to show that the evolution of fainter $\sim 10^{24}$ W radio sources peaks later compared with brighter $\sim 10^{26}$ sources. Rigby et al. (2011) used a tiered sample that included the Waddington et al. (2001) sample and pushed further down to 0.1 mJy at 1.4 GHz (for $z < 1.3$) using photometric redshifts from the Cosmological evolution survey (COSMOS) field. They confirmed this differential evolution with radio luminosity analogous to 'downsizing' seen in star formation rates and X-ray/optical AGN.

The flux range $1 \lesssim S \lesssim 100$ mJy is of particular interest since it samples the RLF in the luminosity regime where the bulk of the energy density from AGN is emitted from redshifts $0.5 \lesssim z \lesssim 3.5$; the peak of AGN activity in the Universe. Hence this flux range is fundamental to our understanding of radio AGN and their impact on their surrounds. Constraining the LF in this parameter space is difficult and has thus far only been possible in small samples with incomplete spectroscopy. In this paper, we look at an alternative approach. We use spectroscopic quasars as a tracer of the large-scale structure at high redshift and cross-correlate these with the NRAO VLA Sky Survey (NVSS) to determine the RLF.

Throughout this work we will assume a standard flat $(\Omega_\mathrm{m}, \Omega_\Lambda) = (0.3, 0.7)$, $h = 0.7$ cosmology. The paper is organized such that we give the background to our technique in Section 2, in Section 3 we introduce the data sets we will be using for our analysis that is described in Section 4. In Section 5, we show our results and discuss their meaning for the RLF in Section 6 and high-redshift clustering in Section 7. We summarize our results in Section 8.

2 REVIEW OF TECHNIQUE

The technique we follow exploits a data set that has redshift information to constrain a sample that does not (Phillipps 1985; Phillipps & Shanks 1987). This approach has been used for many years and has been recently exploited to reproduce the redshift distribution of photometric samples (Newman 2008; Matthews & Newman 2010) and similarly to calibrate photometric redshifts (Schulz 2010). Here, we briefly outline the process we will follow as described in Phillipps (1985) and Phillipps & Shanks (1987).

We begin with the real-space correlation function $\xi(r, z)$ defined such that, for a galaxy population with space density $\phi(L, z)$, the probability of finding a galaxy in a volume δV a distance r from an arbitrary galaxy is

$$\delta P = \phi(L, z)[1 + \xi(L, z, r)]\delta V. \quad (1)$$

In the linear halo–halo regime ($1 \lesssim r \lesssim 100$ Mpc) the correlation function is well described by a power-law $\xi = (r_0/r)^\gamma$ with $\gamma \sim 1.8$ (e.g. Peebles 1980).

The angular statistic Σ_excess is defined as the excess number of galaxies with luminosity L to $L + \delta L$ within a projected radius R of an arbitrary galaxy with known redshift z. Assuming a power-law form for the correlation function, and that the evolution of r_0 and ϕ are minimal over a clustering length

$$\Sigma_\mathrm{excess}(L, z) = \frac{2\pi G(\gamma) r_0^\gamma(L, z) R^{3-\gamma} \phi(L, z)}{3 - \gamma} \delta L, \quad (2)$$

where G is a constant defined by γ (see Phillipps 1985).

Importantly, Σ_excess is trivial to measure between a sample with redshifts and one without. We may then constrain the clustering strength $r_0(z, L)$ and luminosity function $\phi(z, L)$ of a population with no redshifts.

3 DATA

In this paper, we aim to measure the RLF and clustering strength of high-redshift radio sources. We do this by counting quasar–radio source pairs from a spectroscopic quasar sample that has redshifts and a radio catalogue that has none.

We take the NVSS survey (Condon et al. 1998) as our parent sample of radio sources. The NVSS covers the whole sky north of -30°, but for our purposes we are only interested in extragalactic sources and so cut out all objects with galactic latitude $|b| < 10^\circ$ (as well as Dec. < -30). We also make a flux cut at 3 mJy above which the NVSS is $\sim$90 per cent complete (Condon et al. 1998), leaving 1062 117 radio sources in our sample, the vast majority of which have no distance estimate.

The quasar sample we use is a combination of the SDSS DR7 quasar catalogue (Schneider et al. 2010) and the Baryon Oscillation Spectroscopic Survey (BOSS) DR10 quasar catalogue (Pâris et al. 2014). We combine the two samples since they cover different redshift ranges: DR7 $0.1 < z < 2$, DR10 $2 < z < 3.5$. Neither sample has a single consistent selection function and both are somewhat unevenly distributed across the sky. To flatten the DR7 catalogue we follow the simple cut made by Schneider et al. (2010) and only allow objects with $i < 19.1$: the magnitude limit of the main SDSS quasar survey. For the BOSS sample, we make a similar cut of $i < 20$ where the number counts begin to turn over. Further cuts to

these samples are required to construct accurate random catalogues as discussed in the next section.

3.1 Random catalogues

To estimate the excess $\Sigma_{\rm excess}$ we need random catalogues matched to our radio and quasar samples to form a comparison. We create the random radio catalogue by generating random sky positions with Dec. $> -30^\circ$ and $|b| > 10^\circ$. We also assign each source a flux drawn from the NVSS at random. In case of any variation in the flux distribution of the NVSS due to the changing beam with declination we discretize the NVSS catalogue into one degree declination strips and only draw a flux value for our random source from objects within the same declination strip.

To create the random quasar catalogue we use MANGLE and the 'SDSS DR72' radial selection function from the mangle website (Hamilton & Tegmark 2004; Blanton et al. 2005; Swanson et al. 2008). Note that the DR72 mask was developed to reproduce the sky coverage of the main DR7 spectroscopic galaxy survey, and does not include additional fields that were in the DR7 quasar catalogue. Therefore, we apply this mask to cut the area of our real DR7 quasar catalogue as well. We then produce a random catalogue from the DR72 mask with 10 times the number of random objects as quasars.

To make the random BOSS DR10 sample we again use MANGLE and the same DR72 mask. Note that this mask does not include approximately a quarter of the BOSS survey that was only covered photometrically after DR7. However, the DR72 mask reproduces the small-scale coverage of the survey and so we accept this loss of objects.

To cut the DR72 area to just that observed by BOSS we take the field centres of the spectroscopic observations from the SDSS website and only include objects within 1.°49 of a field centre. Again, we produce this random catalogue with ten times the number of objects as BOSS quasars.

Our final quasar catalogue has 80 494 objects, 63 682 from DR7 and 16 812 from DR10. Fig. 1 shows the redshift distributions of the final samples split by their survey. Clearly the inclusion of the BOSS DR10 quasars extends the redshift coverage of our sample

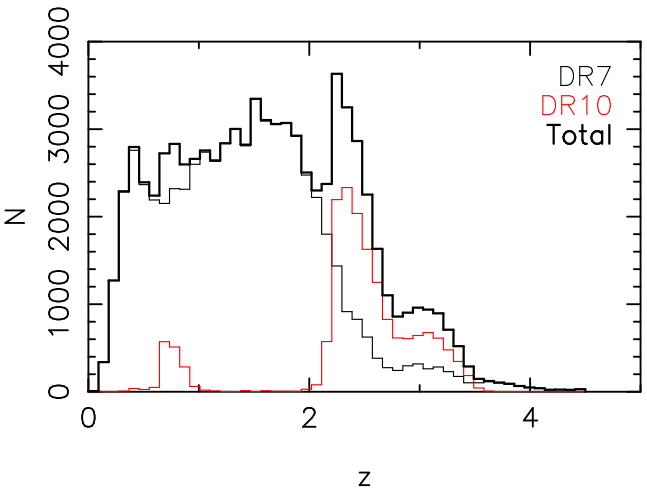

Figure 1. The redshift distribution of our final quasar sample. The fine lines show the DR7 (black) and DR10 (grey/red) samples separately and the heavy line shows the total. This demonstrates the extra redshift range from $z \sim 2$ to 3.5 made available by the inclusion of the DR10 quasars.

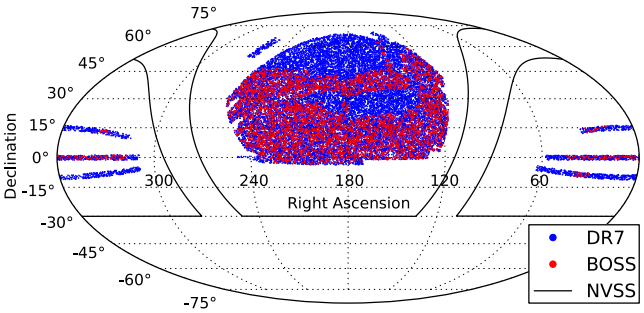

Figure 2. The distribution of our final quasar samples in the sky. Red and Blue are the SDSS DR7 and BOSS samples respectively while the black line shows the Dec.$> -30^\circ$ and galactic $|b| > 10^\circ$ cuts that define the NVSS area we consider.

from $z \sim 2.2$ to 3.5. The distribution of these quasars on the sky along with the NVSS boundaries are shown in Fig. 2.

4 ANALYSIS

The excess number of radio sources around quasars at a given redshift and radio luminosity (calculated assuming the redshift of the quasar), $\Sigma_{\rm QR}(z, L)$, constrains the cross-clustering strength $r_{0\rm QR}(z, L)$ and the RLF $\phi(z, L)$ (equation 2). By assuming prior knowledge of either $r_{0\rm QR}$ or ϕ we can then constrain the other. In this section, we describe models we will assume for $r_{0\rm QR}$ and our method for estimating Σ.

4.1 The clustering strength of quasars and radio sources

In reality the cross-clustering strength $r_{0\rm QR}$ that appears in equation (2) is rarely measured. More commonly the autocorrelation strengths of quasars, $r_{0\rm QQ}$, or radio sources, $r_{0\rm RR}$, are studied. We will relate these quantities by assuming linear bias such that $r^2_{0\rm QR} \sim r_{0\rm QQ} \times r_{0\rm RR}$ (e.g. Wake et al. 2008a) and model $r_{0\rm QQ}$ and $r_{0\rm RR}$ as a function of redshift and luminosity based on recent analyses.

Studies of quasar clustering have repeatedly shown that the quasar correlation function is roughly independent of quasar luminosity (da Ângela et al. 2008; Shanks et al. 2011). $r_{0\rm QQ}$ increases slowly with redshift and, since the mass clustering is falling as redshift increases, the quasar bias rises quickly with redshift. Converting bias into mass via Press–Schechter theory implies that the average dark halo mass of quasars is roughly constant with $M_{\rm DH} \sim 10^{12}\,{\rm M}_\odot$ at all redshifts (Croom et al. 2005; Myers et al. 2006; Ross et al. 2009).

Assuming there is no variation in quasar clustering strength with luminosity we only need the variation with redshift. Fig. 3 shows the autocorrelation clustering strength of quasars as a function of redshift from Ross et al. (2009). We perform a χ^2 minimization for evolution of the clustering strength assuming the quadratic form

$$r_0 = a + bz^2, \tag{3}$$

where r_0 has units of Mpc assuming $h = 0.7$. We find $a = 6.8 \pm 0.31$ and $b = 0.63 \pm 0.26$. We will use this empirical fit to estimate $r_{0\rm QQ}(z)$.

The clustering of mJy radio sources has been extensively studied at redshifts below $\sim$0.8 with samples cross-matched to optical spectroscopic or photometric galaxies (Peacock & Nicholson 1991; Brand et al. 2005; Wake et al. 2008b; Donoso et al. 2010; Fine et al. 2011; Lindsay et al. 2014a). At the radio luminosities sampled in those surveys ($L \gtrsim 10^{24}$ W Hz^{-1}) the radio population is dominated

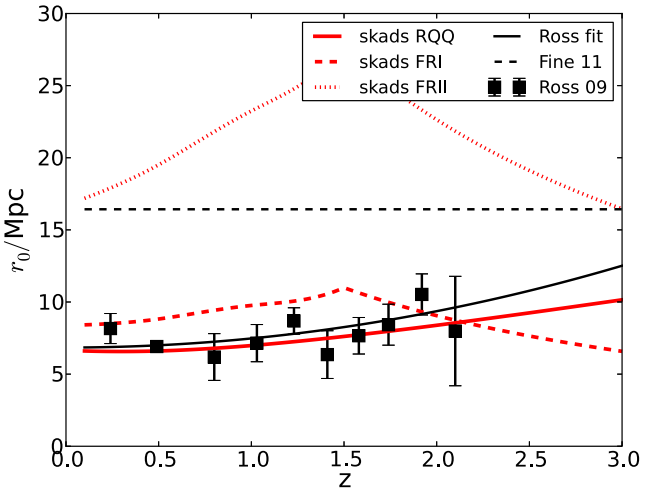

Figure 3. The clustering strengths (r_0) for the populations we are considering. Black points give the quasar autocorrelation strength from Ross et al. (2009) and the solid line is our simple fit to these. The dashed black line gives the constant radio galaxy autocorrelation strength from Fine et al. (2011). Grey lines show the correlations strengths assumed in the W08: solid radio-quiet quasars, dashed FR Is and dotted FR IIs.

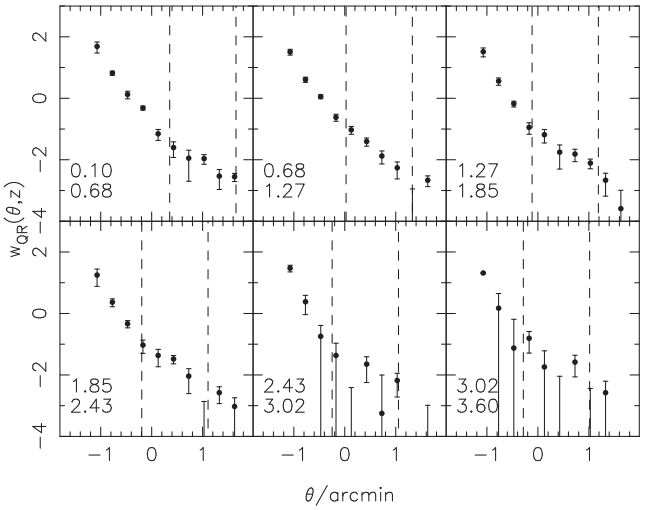

Figure 4. The quasar–radio source angular correlation function of our sample. The vertical lines are at 2 and 20 Mpc projected distance. The redshift limits for each bin are given in the bottom left of the panels.

by AGN typically hosted by LRGs. Fine et al. (2011) showed little evolution in the clustering strength of these objects with a constant $r_{0RR} \sim 11.5\,h^{-1}$ Mpc (Fine et al. 2011). This broadly matches the lack of clustering evolution seen in optically selected LRGs (Bell et al. 2004; Wake et al. 2006; Brown et al. 2007). At redshifts greater than 0.8 there are few indications of the clustering of radio sources due to the lack of wide-field optical galaxy samples in this redshift regime. Lindsay, Jarvis & McAlpine (2014b) used photometric galaxy sample over a small field with deep radio observations to measure the cross-correlation with IR galaxies. They found no variation in clustering strength with radio power and while their correlation increased with redshift this is primarily driven by evolution in their IR galaxy sample rather than the radio.

The dependence of clustering strength on radio luminosity is not well described. In their angular correlation analysis of the NVSS Overzier et al. (2003) derived a correlation scalelength of $r_{0RR} \sim 6\,h^{-1}$ Mpc for lower luminosity sources $\lesssim 10^{26}$ W Hz^{-1} while the brighter, potentially FR II, sources had a scalelength $r_{0RR} \sim 14\,h^{-1}$ Mpc. On the other hand clustering analyses of radio surveys matched to optical galaxies have found no luminosity dependence in the large-scale halo–halo regime (Donoso et al. 2010; Fine et al. 2011; Lindsay et al. 2014b). Note that since the Overzier et al. (2003) had no redshift information a considerable series of assumptions about the radio population were required to derive their result, on the other hand both Donoso et al. (2010) and Fine et al. (2011) struggled for sources in their samples with $L > 10^{26}$ W Hz^{-1} while Lindsay et al. (2014b) had none.

Given the few constraints on r_{0RR} we initially make the simplest empirical assumption. That is the clustering strength of our radio sample is constant with redshift and luminosity with $r_{0RR} = 11.5\,h^{-1}$ Mpc. Assuming linear bias and $r_{0QQ}(z)$ from Ross et al. (2009) this makes up our empirical (EMP) model for $r_{0QR}(L, z)$.

As an alternative and check we also consider the values assumed in Wilman et al. (2008, hereafter W08) when they were attempting to model the radio sky. They followed Overzier et al. (2003) and assumed considerably stronger clustering for the brightest radio sources. For $z < 1.5$ they assumed constant dark halo masses of 10^{13} and $10^{14}\,h^{-1}$ M$_\odot$ for FR I and FR II sources, respectively. At high redshift the clustering strength of their FR II sources would become unphysically large and so for $z > 1.5$ they held the bias of their FR I and FR II sources constant. We make the simplistic assumption that all radio sources with $L < 10^{26}$ W Hz^{-1} are FR I sources, the rest being FR IIs. For radio-quiet AGN, essentially quasars, they assumed a constant halo mass of $3 \times 10^{12}\,h^{-1}$ M$_\odot$ with a similar redshift cut at $z = 3$ above which the bias was held constant. We will refer to this alternative model for r_{0QR} as the W08 model (see Fig. 3 for a comparison of the differing models).

4.2 Removing radio-loud quasars

The statistic $\Sigma_{\rm excess}$ defined in Section 2 is the excess number of radio sources around quasars. In the derivation of equation (2) it is assumed that this excess comes only from the clustering of matter. Radio-loud quasars in our sample increase the measured Σ and bias our results. To illustrate this effect Fig. 4 shows the angular cross-correlation function $w_{QR}(\theta, z)$ for our sample of quasars (split into redshift bins) and the NVSS catalogue. The vertical lines in the figure show 2 and 20 Mpc projected on to the angular scale at the redshift of the bins. The upturn below ∼2 Mpc is caused by a combination of radio-loud quasars and non-linear single halo clustering (e.g. Blake & Wall 2002). We remove the radio-loud contribution by only counting pairs in the annulus between $R = 2$ and 20 Mpc. In this region, the angular correlation function is well fit by a single power law indicating that the spatial correlation function $\xi(r)$ is also approximately a power law. We choose 2 Mpc as the lower limit both from inspection of Fig. 4 and since this corresponds to roughly the largest known giant radio galaxies (Saripalli et al. 2005).

4.3 Calculating Σ

To estimate Σ we count all radio sources with a projected distance between 2 and 20 Mpc from a quasar in our samples, $N_{\rm DD}$. In addition to these data-data pairs we also substitute our random catalogues and count $N_{\rm DR}$, $N_{\rm RD}$ and $N_{\rm RR}$. This is done in redshift and luminosity bins, where the luminosity of the radio sources are calculated assuming the redshift of the quasar. Redshift bins are equally

spaced over the interval sampled by our quasars $0.1 < z < 3.6$. Luminosity bins are logarithmically spaced over three orders of magnitude, the lower limit of which is the lowest luminosity observable in that redshift bin. The flux limit of the NVSS catalogue gives a Malmquist bias. Hence in our summations each pair is weighted by $V_{\rm bin}/V_{\rm max}$.

Following Hamilton (1993) we estimate Σ with

$$\Sigma = \frac{1}{N_Q}(N_{\rm DD} - N_{\rm RR}N_{\rm DR}/N_{\rm RD}), \quad (4)$$

where N_Q is the total number of quasars in the redshift bin. From equation (2) we relate Σ to the luminosity function and clustering strength with

$$\Sigma_{\rm excess}(L,z) = \frac{2\pi G(\gamma) r_0^{\gamma}(L,z)(R_{\rm max}^{3-\gamma} - R_{\rm min}^{3-\gamma})\phi(L,z)}{3-\gamma}\delta L. \quad (5)$$

Throughout this paper, we will assume $\gamma = 1.8$ hence $G = 3.678$, and use $R_{\rm max}$, $R_{\rm min} = 20$, 2 Mpc. Equation (5) becomes

$$\Sigma_{\rm excess}(L,z) = 657 r_{0{\rm QR}}^{1.8}(L,z)\phi(L,z)\delta L. \quad (6)$$

We assume this simple relationship between Σ, r_0 and ϕ throughout the rest of this work.

We use jackknife resampling to estimate our errors by splitting our sample into 20 even sized (by number of quasars) subfields by right ascension. We then calculate Σ in each subfield and estimate the 'field-to-field' errors from the rms of these values for Σ (e.g. Fine et al. 2011; Sawangwit et al. 2011).

5 EXCESS PAIR COUNTS

Fig. 5 shows the values of $\Sigma_{\rm excess}$ we calculate from our sample for six redshift and five luminosity bins. The way Σ is calculated means that it can be scattered to negative values due to noise. Hence we show both a linear and logarithmic scale to illustrate how the measured values and their errors behave. The points with $\Sigma < 0$ and their errors still contain information about our sample and need to be included in any analysis to avoid introducing bias. Furthermore, the error bars are symmetric and approximately Gaussian in linear space. Hence, while plots may be in log space, any fitting to the data is performed in linear space.

It is apparent from Fig. 5 that at fixed radio luminosity $\Sigma(L, z)$ increases slightly with redshift. This indicates that one of $r_{0\rm QR}$ or ϕ is increasing with redshift.

6 THE RADIO LUMINOSITY FUNCTION

Fig. 6 shows the RLF we calculate for six redshift bins. We show the LF calculated assuming the EMP (solid points) and W08 (open points) clustering models. There is very little overall difference in the LFs between the clustering models. The solid lines in Fig. 6 show the Willott et al. (2001) RLF model at the mid-point redshift of the bin and it is clear that in general our results are consistent with their model.

To describe our data further we initially fit an evolving power-law $\phi = A(1+z)^{\alpha}(L/10^{26})^{\beta}$ and find $\alpha = 1.00 \pm 0.35$ for the EMP model and 1.02 ± 1.05 for W08. However, we find the large redshift and flux range we sample mean this is not an accurate model for our data. To better illustrate the redshift evolution in our data we fix the luminosity exponent to that from our fit ($\beta = -0.99$EMP; -0.85 W08) and just fit for the amplitude of the power law in each redshift bin. Fig. 7 shows the amplitude of the fitted power law at 10^{26} W Hz^{-1} as a function of redshift.

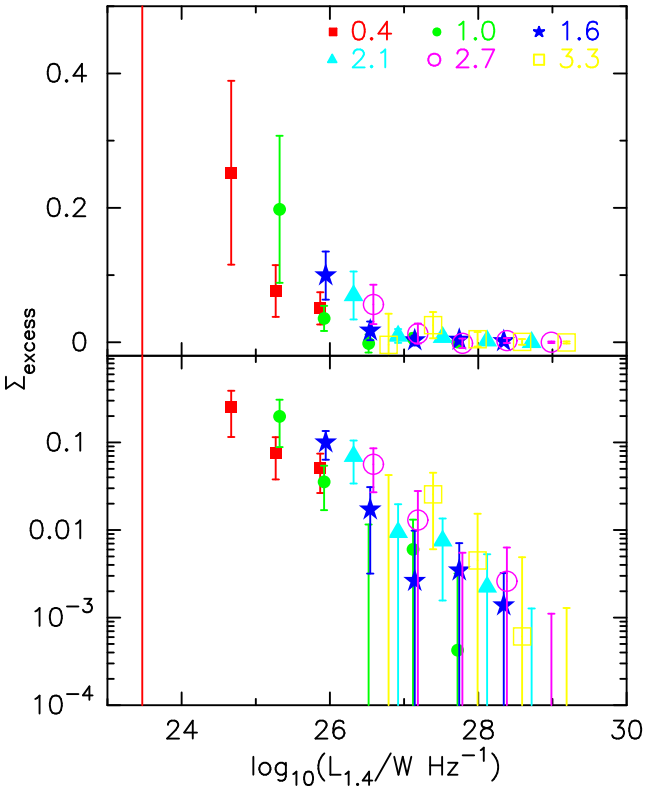

Figure 5. The average excess of radio sources around quasars, Σ, binned by redshift and luminosity. We show the plot with both a linear and logarithmic scale since several of the points are scattered below $\Sigma = 0$ by noise.

6.1 Redshift cut-off

Fig. 7 indicates that the increase in space density slows and may turnover at higher redshifts. To include this behaviour we introduce a redshift limit and separate parameter for high-redshift evolution

$$\Phi(L,z) = \begin{cases} (1+z)^{\alpha_l}(L/10^{26})^{\beta} & z \le z_{\rm lim} \\ (1+z_{\rm lim})^{\alpha_l-\alpha_h}(1+z)^{\alpha_h}(L/10^{26})^{\beta} & z > z_{\rm lim}, \end{cases} \quad (7)$$

where α_h and α_l are the evolution parameters above and below $z_{\rm lim}$. Since there can be relatively rapid evolution we bin our data into 25 redshift and 10 luminosity bins. We fit our model with simple Markov chain Monte Carlo (MCMC) routine iterated 500 000 times to find the preferred values. We fix $\beta = -1$ in the fitting since there can be a degeneracy between the evolution parameter and β due to our LFs being defined in different parts of luminosity space at different redshifts. Fig. 8 shows the probability distributions from our fitting using the EMP model, along with the best-fitting values. Clearly our data support strong $\alpha_h \sim 4$ evolution up to $z_{\rm lim} \sim 2$. At high redshift we only have an upper limit on the evolution parameter but can show at least that the increase in space density stops, or turns over. Interestingly, this redshift cut-off is almost identical to that found by Willott et al. (2001) for their high-luminosity objects $z_{\rm cut-off} = 1.91 \pm 0.16$.

To compare further with Willott et al. (2001) we fitted out data using a parametrization based on their models. Their model 'C' is split into two populations roughly separated at $L = 26$ W Hz^{-1}. We fit for $(1+z)^{\alpha}$ evolution with a redshift cut as in equation (7) for each population. In this fitting, we convert from their cosmology to our own to make the fitted values comparable. In the high-luminosity regime we have very few quasar-radio source pairs and consequently

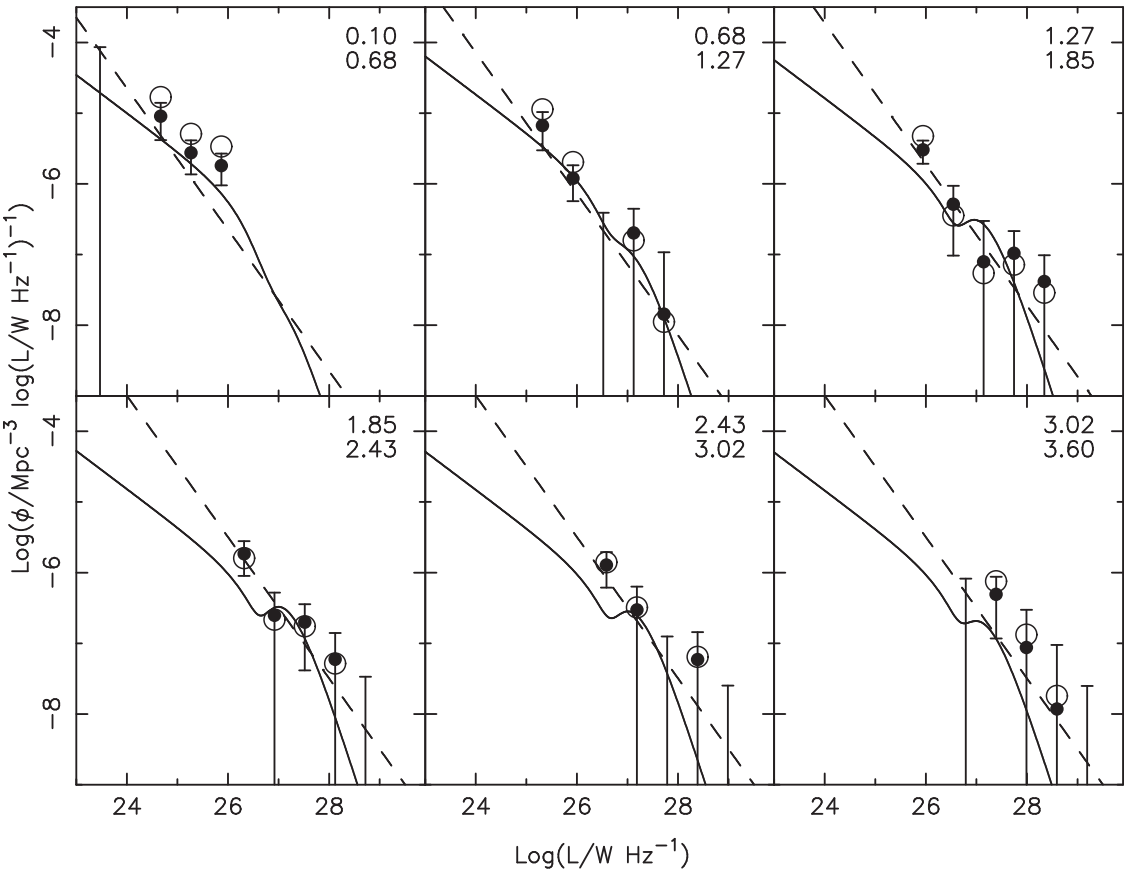

Figure 6. The RLF. Solid points assume the EMP clustering model while open points are W08. The solid line shows the Willott et al. (2001) RLF model and the dashed line shows our evolving power-law model fit to the data at the mid-points of the bin (top right in each panel). The redshift range for each bin is given at the top right of each panel. The poor fit in the first redshift bin is due to the data being dominated by radio sources at the high-z limit of the bin.

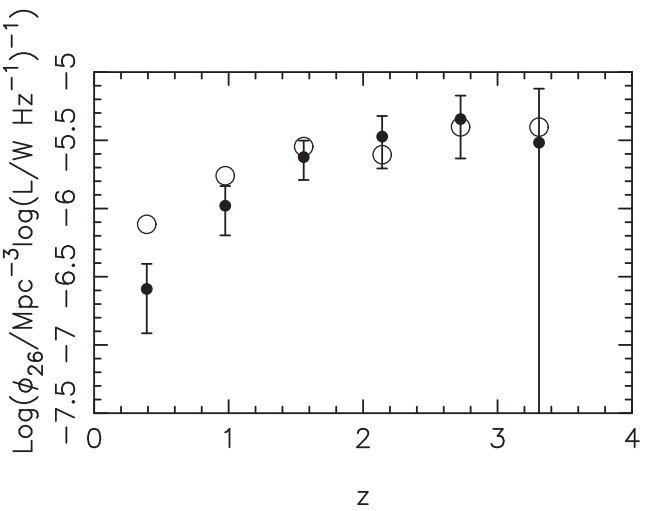

Figure 7. The evolution of the amplitude of the RLF from $z \sim 3.5$. The solid points are using the EMP model, the open points W08.

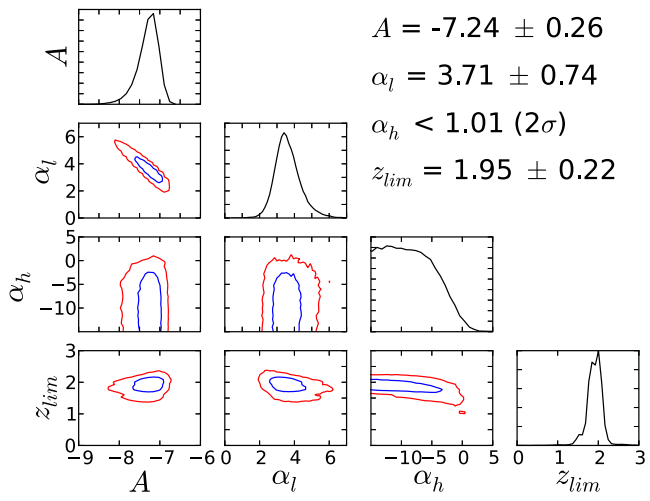

Figure 8. The results of our MCMC fitting of our RLF data. Blue and red lines show the 1σ and 2σ marginalized constraints, respectively. We constrain all but the high-redshift evolution parameter for which we can only obtain an upper limit.

this part of parameter space is poorly constrained. On the other hand, at low luminosities we find $(1 + z)^{2.35 \pm 0.89}$ evolution to redshift 1.94 ± 0.43 above which we can only estimate an upper limit for the evolution parameter $\alpha_h < 1.3$ (2σ). This contrasts with their findings of $\alpha_l = 3.5$ up to a redshift cut-off at 0.7. Willott et al. (2001) have a considerably brighter sample than we use here and their redshift cut is imposed by their flux limit. It may be that since we are able to better define $z_{\rm cut}$ this explains the smaller discrepancy between our evolution parameters.

6.2 Discussion

Our results are consistent with a model that evolves strongly, $\Phi \propto (1+z)^{3.7}$, to $z \sim 2$ above which the LF either stays constant or falls. Interestingly, this is approximately the same redshift evolution that Willott et al. (2001) found for their high-luminosity population of sources. The indication is that, rather than having two separate populations with a transition at $L \sim 10^{26}$ W, the radio LF may be dominated by a single population in the luminosity–redshift regime we are sampling.

Recent studies of the RLF have focused on the accretion mechanisms that launch the radio jet and the role that the AGN may play in heating the intergalactic medium. Terminologies differ but we will refer to high-excitation radio galaxies (HERGs) associated with high accretion rate optical AGN and low-excitation radio galaxies (LERGs) associated with substantially lower accretion rates via advection-dominated accretion flows in massive elliptical galaxies. At low redshifts, LERGs dominate the LF below $L \sim 10^{26}$ W (Hardcastle, Evans & Croston 2007; Best & Heckman 2012). At these fainter luminosities and lower redshifts the LF has been shown to only evolve slowly (Clewley & Jarvis 2004; Sadler et al. 2007; Smolčić et al. 2009; McAlpine et al. 2013). However, there is evidence that the HERG population evolves considerably more strongly than the LERGs (Willott et al. 2001; Best et al. 2014), potentially becoming the dominant population in the luminosity range we sample around $z \sim 1$.

The 3 mJy flux limit we impose allows us to sample luminosities of 10^{26} W up to $z = 2.5$. However, the strong evolution of the LF coupled with the increased comoving volume at high redshift means that we are dominated by sources at $z \sim 2$. Assuming the simplistic power-law LF from our MCMC fit, less than 5 per cent of our sample is at $z < 1$. The indication is that our signal is dominated by HERGs, and hence it may be unsurprising that we find almost identical evolution parameters to the factor of ∼50 brighter Willott et al. (2001) sample.

Waddington et al. (2001) and Rigby et al. (2011) found that the fainter end of the RLF peaked in density at lower redshift. Due to the nature of our analysis we are always dominated by the radio sources close to our flux limit. Hence, we cannot split the sample into luminosity bins to compare across a range of redshifts. We find a redshift cut-off at $z = 1.95 \pm 0.22$. At this redshift our 3 mJy flux limit translates to $\log(L/\mathrm{W}) = 25.77$, and so we can consider the turnover seen in our data to be due to radio sources at or somewhat brighter than this. At these luminosities Rigby et al. (2011) found a redshift cut closer to $z = 1$ although our results are consistent within a few sigma.

7 THE CLUSTERING OF RADIO SOURCES

Reversing what we have done above we can integrate the Willott et al. (2001) luminosity function above our flux limit to give ϕ in equation (6) and hence constrain the clustering strength between the radio sources and quasars in our sample. Fig. 9 shows the measured cross-correlation strength in six redshift bins. While there may be some hint of an increase in clustering strength with z, $r_{0\mathrm{QR}}$ is consistent with a constant value of 10.4 ± 2.5 Mpc over the full redshift range sampled (if poorly constrained at the highest redshifts). The dashed line in Fig. 9 shows the value of $r_{0\mathrm{RR}}$ assuming the empirical fit in Fig. 3 and $r_{0\mathrm{QR}}^2 = r_{0\mathrm{QQ}} r_{0\mathrm{RR}}$. Again the estimates for $r_{0\mathrm{RR}}$ are consistent with a constant value of 15.4.

At lower redshift ($z < 1.5$) we find considerably stronger clustering in our sample compared to quasars, more in line with the results for radio galaxies from Fine et al. (2011) and Lindsay et al. (2014a). At higher redshifts both our errors and the clustering strength of quasars increase and we cannot form a distinction.

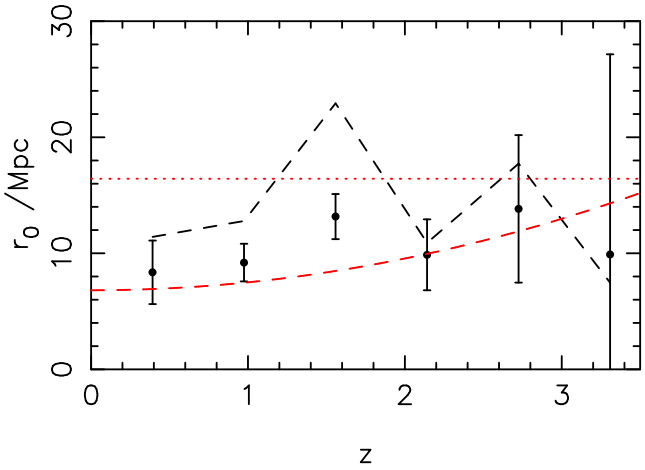

Figure 9. The points with error bars show $r_{0\mathrm{QR}}$ as a function of redshift for our sample. The dashed black line gives the implied value of $r_{0\mathrm{RR}}$ assuming the empirical values of $r_{0\mathrm{QQ}}$ from (Ross et al. 2009). Grey dashed and dotted lines show our EMP model values for $r_{0\mathrm{QQ}}$ and $r_{0\mathrm{RR}}$, respectively.

Our results for $r_{0\mathrm{RR}}$ are not consistent with the strong 20–25 Mpc values assumed in W08 for FR II sources. This is despite our being dominated by bright $L > 10^{26}$ W sources at high redshift and our sample potentially being dominated by HERGs/FR IIs at all redshift as discussed in our RLF analysis. None the less, we find are strong enough clustering to indicate these radio sources are in some of the most massive haloes at all redshifts we sample ($\sim 10^{14}$ $\mathrm{M}_\odot$ at $z \sim 0$ to $\sim 10^{12.5}$ $\mathrm{M}_\odot$ at $z \sim 3$). A possible explanation for this would be a later ($z < 1.5$) break imposed in the W08 bias/clustering model, combined with our being dominated by fainter FR I/LERG sources at low redshift. Alternatively, the clustering strength could depend strongly on luminosity and redshift to contrive to give our results, although this has not been noted before.

8 SUMMARY

We measure the overdensity $\Sigma(z, L)$ of radio sources around spectroscopic quasars and relate this to evolution in the radio source population from $z \sim 3.5$ to today. Our key results can be summarized as follows.

$\Sigma(z, L)$ is measured in redshift/luminosity bins and we find significant evolution with redshift. This can only be explained by either the RLF of clustering strength increasing to $z \sim 2$.

Under some simple models for $r_0(z, L)$ we find strong evolution, $\phi \propto (1+z)^{3.7 \pm 0.7}$, up to $z = 1.9 \pm 0.2$ above which the evolution declines, although we can only constrain an upper limit. These evolution parameters are consistent with those found by Willott et al. (2001) for the brighter radio source population. The indication may be that the same population of HERGs dominates the NVSS at all flux densities above $z \sim 1$.

Assuming the Willott et al. (2001) LF model we find the clustering strength of radio sources to be consistent with a value of $r_{0\mathrm{RR}} = 15.0 \pm 2.5$. This is inconsistent with quasars at low redshift and the W08 model for FR II clustering at intermediate ($1 \lesssim z \lesssim 2$). A possible explanation would be the population being dominated by LERGs at low redshift and clustering more like quasars at higher

redshift. Regardless, our results show that these radio sources are found in the most massive dark matter haloes at all redshift we sample.

In this work, we have demonstrated a technique that exploits a well-defined sample with distance information to constrain the luminosity function and clustering of a sample without. The next generation of radio surveys will push still deeper beyond the flux limits of the NVSS used here. Despite new wide-field redshift surveys (e.g. *Euclid*) the vast majority of the sources detected in these surveys will not have reliable distances. The method presented in this work offers an alternative approach to studying these populations with observational strategies that are already possible and, for the most part, have already been carried out.

ACKNOWLEDGEMENTS

SF and RJ would like to acknowledge SKA South Africa and the NRF for their funding support.

REFERENCES

Bell E. F. et al., 2004, ApJ, 608, 752
Best P. N., Heckman T. M., 2012, MNRAS, 421, 1569
Best P. N., Kauffmann G., Heckman T. M., Ivezić Ž., 2005, MNRAS, 362, 9
Best P. N., Ker L. M., Simpson C., Rigby E. E., Sabater J., 2014, MNRAS, 445, 955
Blake C., Wall J., 2002, MNRAS, 329, L37
Blanton M. R. et al., 2005, AJ, 129, 2562
Boyle B. J., Shanks T., Croom S. M., Smith R. J., Miller L., Loaring N., Heymans C., 2000, MNRAS, 317, 1014
Brand K., Rawlings S., Hill G. J., Tufts J. R., 2005, MNRAS, 357, 1231
Brown M. J. I., Dey A., Jannuzi B. T., Brand K., Benson A. J., Brodwin M., Croton D. J., Eisenhardt P. R., 2007, ApJ, 654, 858
Cannon R. et al., 2006, MNRAS, 372, 425
Clewley L., Jarvis M. J., 2004, MNRAS, 352, 909
Condon J. J., Broderick J. J., 1988, AJ, 96, 30
Condon J. J., Cotton W. D., Greisen E. W., Yin Q. F., Perley R. A., Taylor G. B., Broderick J. J., 1998, AJ, 115, 1693
Croom S. M. et al., 2005, MNRAS, 356, 415
da Ângela J. et al., 2008, MNRAS, 383, 565
Donoso E., Li C., Kauffmann G., Best P. N., Heckman T. M., 2010, MNRAS, 407, 1078
Dunlop J. S., Peacock J. A., 1990, MNRAS, 247, 19
Eisenstein D. J. et al., 2001, AJ, 122, 2267
Fine S., Shanks T., Nikoloudakis N., Sawangwit U., 2011, MNRAS, 418, 2251
Hamilton A. J. S., 1993, ApJ, 417, 19
Hamilton A. J. S., Tegmark M., 2004, MNRAS, 349, 115
Hardcastle M. J., Evans D. A., Croston J. H., 2007, MNRAS, 376, 1849
Jarvis M. J., Rawlings S., 2004, New Astron. Rev., 48, 1173
Lindsay S. N. et al., 2014a, MNRAS, 440, 1527
Lindsay S. N., Jarvis M. J., McAlpine K., 2014b, MNRAS, 440, 2322
McAlpine K., Jarvis M. J., Bonfield D. G., 2013, MNRAS, 436, 1084
Matthews D. J., Newman J. A., 2010, ApJ, 721, 456
Mauch T., Sadler E. M., 2007, MNRAS, 375, 931
Mauch T., Murphy T., Buttery H. J., Curran J., Hunstead R. W., Piestrzynski B., Robertson J. G., Sadler E. M., 2003, MNRAS, 342, 1117
Myers A. D. et al., 2006, ApJ, 638, 622
Newman J. A., 2008, ApJ, 684, 88
Overzier R. A., Röttgering H. J. A., Rengelink R. B., Wilman R. J., 2003, A&A, 405, 53
Padovani P., Mainieri V., Tozzi P., Kellermann K. I., Fomalont E. B., Miller N., Rosati P., Shaver P., 2009, ApJ, 694, 235
Padovani P., Miller N., Kellermann K. I., Mainieri V., Rosati P., Tozzi P., 2011, ApJ, 740, 20
Pâris I. et al., 2014, A&A, 563, A54
Peacock J. A., Nicholson D., 1991, MNRAS, 253, 307
Peebles P. J. E., 1980, The Large-scale Structure of the Universe, Princeton Univ. Press, Princeton, NJ
Phillipps S., 1985, MNRAS, 212, 657
Phillipps S., Shanks T., 1987, MNRAS, 227, 115
Rigby E. E., Best P. N., Brookes M. H., Peacock J. A., Dunlop J. S., Röttgering H. J. A., Wall J. V., Ker L., 2011, MNRAS, 416, 1900
Ross N. P. et al., 2009, ApJ, 697, 1634
Sadler E. M. et al., 2007, MNRAS, 381, 211
Saripalli L., Hunstead R. W., Subrahmanyan R., Boyce E., 2005, AJ, 130, 896
Sawangwit U., Shanks T., Abdalla F. B., Cannon R. D., Croom S. M., Edge A. C., Ross N. P., Wake D. A., 2011, MNRAS, 416, 3033
Schneider D. P. et al., 2010, AJ, 139, 2360
Schulz A. E., 2010, ApJ, 724, 1305
Seymour N. et al., 2008, MNRAS, 386, 1695
Shanks T., Croom S. M., Fine S., Ross N. P., Sawangwit U., 2011, MNRAS, 416, 650
Simpson C. et al., 2006, MNRAS, 372, 741
Smolčić V. et al., 2009, ApJ, 696, 24
Swanson M. E. C., Tegmark M., Hamilton A. J. S., Hill J. C., 2008, MNRAS, 387, 1391
Waddington I., Dunlop J. S., Peacock J. A., Windhorst R. A., 2001, MNRAS, 328, 882
Wake D. A. et al., 2006, MNRAS, 372, 537
Wake D. A. et al., 2008a, MNRAS, 387, 1045
Wake D. A., Croom S. M., Sadler E. M., Johnston H. M., 2008b, MNRAS, 391, 1674
Willott C. J., Rawlings S., Blundell K. M., Lacy M., Eales S. A., 2001, MNRAS, 322, 536
Wilman R. J. et al., 2008, MNRAS, 388, 1335 (W08)

This paper has been typeset from a TEX/LATEX file prepared by the author.